Conserved Peroxiporin Function in MIP Channels: Structural and Thermodynamical Insights.

Jonathan Chevriau[1,2] , Gerardo Zerbetto De Palma[1,2] , Ari Zeida[3] , Karina Alleva[1,2]
1) Universidad de Buenos Aires, Facultad de Farmacia y Bioquímica, Departamento de Fisicomatemática, Cátedra de Física, Argentina.
2) IQUIFIB, UBA-CONICET, Argentina
3)Departamento de Bioquímica y Centro de Investigaciones Biomédicas (Ceinbio), Facultad de Medicina, Universidad de la República, Uruguay

The Membrane Intrinsic Protein (MIP) family plays a crucial role in facilitating the transport of water and small solutes across biological membranes, including hydrogen peroxide (H_2O_2). However, the evolutionary origin of H_2O_2 transport within the MIP family remains unclear, with the possibility that this function could be an ancestral trait. MIPs that are capable of transporting H_2O_2 are referred to as peroxiporins. It is important to note that not all MIPs, even those that are closely related, exhibit H_2O_2 permeability. The molecular determinants that govern H_2O_2 permeation and selectivity are not yet fully understood. Our previous studies have provided valuable insights into the transport mechanism of the MtPIP2;3 protein

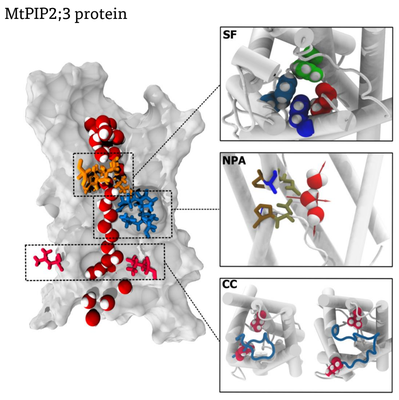

Constriction regions in MIPs

Selectivity Filter (SF):
- Composed of amino acids that form a structure selective for specific molecules (e.g., water).
- Selectivity varies across MIP types, influencing permeability.

NPA Region:
- Contains two conserved NPA motifs forming loops near the SF.
- Critical for pore formation and molecule selectivity.

Cytoplasmic Filter:
- Found in gated aquaporins like PIPs.
- Conformational rearrangement blocks water transport.

It is unclear whether peroxiporin activity is conserved across all MIP subfamilies or arose through lineage-specific diversification

To assess the conservation of the H_2O_2 permeation mechanism observed in *Mt*PIP2;3 and to investigate the structural determinants of H_2O_2 permeability, we extended our analysis to a diverse set of MIP channels representing the four major eukaryotic evolutionary groups (AQP1-like, AQP3-like, AQP8-like, and AQP11-like). This comparative analysis included both experimentally validated H_2O_2 transporters and non-transporters, as well as their human and plant homologs.

Case study: *Mt*PIP2;3

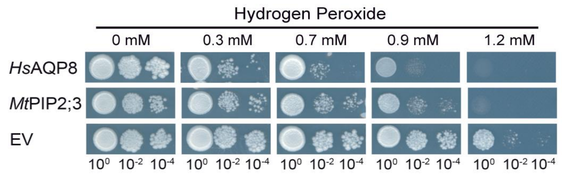

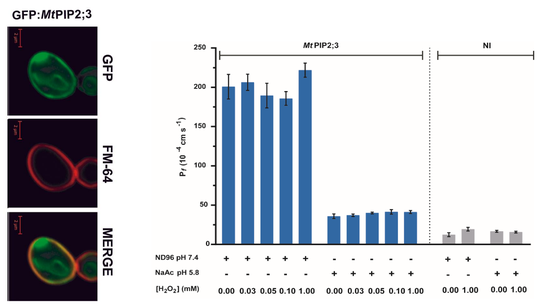

MtPIP2;3 H_2O_2 transport
- MtPIP2;3 expressed in *Saccharomyces cerevisiae* localizes to the plasma membrane.
- Capable of transporting hydrogen peroxide (**peroxiporin**).

Impact of H_2O_2 on water transport
- MtPIP2;3 is highly efficient in water transport.
- Heterologous system (*Xenopus laevis* oocytes) used to study H_2O_2 effects on MtPIP2;3.
- H_2O_2 does not alter water permeability of MtPIP2;3 in either open or closed state.
- No direct regulatory effect of H_2O_2 on water transport.

Model characterization
- Open/closed states identified in molecular dynamics simulations.
- H_2O_2 addition had no impact on protein conformations.
- Main difference: closed state has narrower pore due to leucine protrusion from loop D.
- Permeability events occur in open chains, but no molecule passage in closed chains, despite H_2O_2 presence.

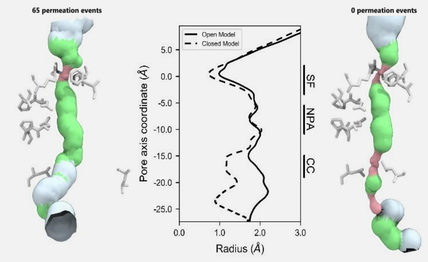

- **H_2O vs H_2O_2 Distribution**:
  - H_2O is uniformly distributed along the pore in both conformations.
  - H_2O_2 shows preference for specific areas:
    - NPA region excludes H_2O_2, but H_2O is distributed normally.
    - In the closed state, H_2O_2 presence in SF, NPA, and CC regions is negligible.
- **Permeation Energy**:
  - Both molecules face a major energy barrier around the SF region in the open state (~4 kcal/mol).
  - In the open state, H_2O_2 experiences a free energy increase (~1 kcal/mol) in the NPA region, unlike H_2O.
  - In the closed state, energy barriers are higher for both molecules (~8 kcal/mol for H_2O_2).
  - Lower energy between NPA and CC, but increases near the pore end in both states, trapping molecules and hindering passage.

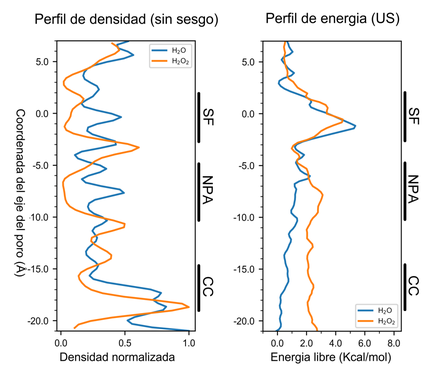

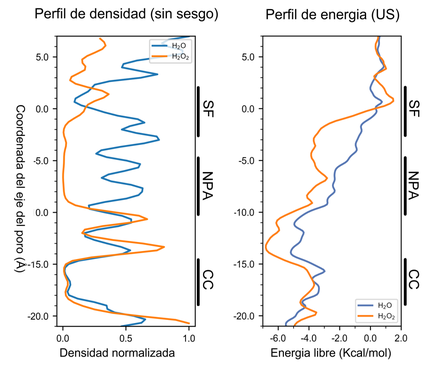

AQP1-Like

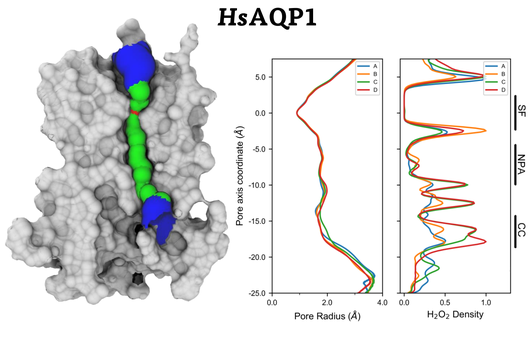

AQP3-Like

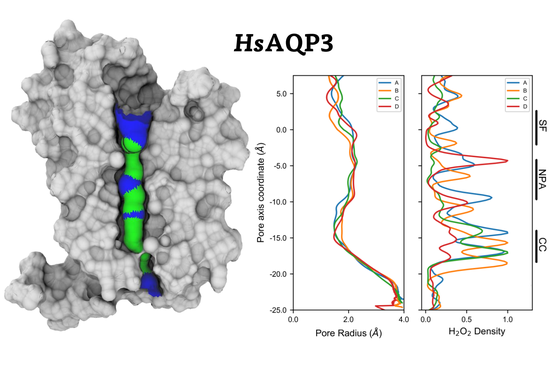

AQP11-Like

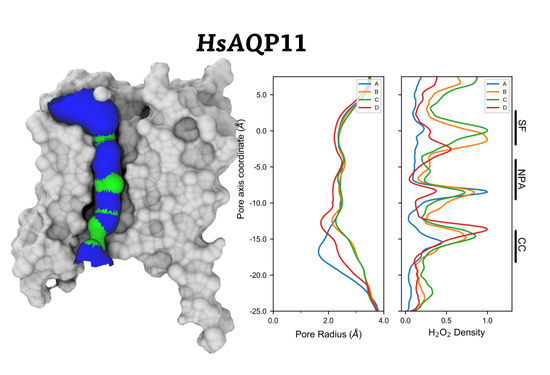

AQP8-Like

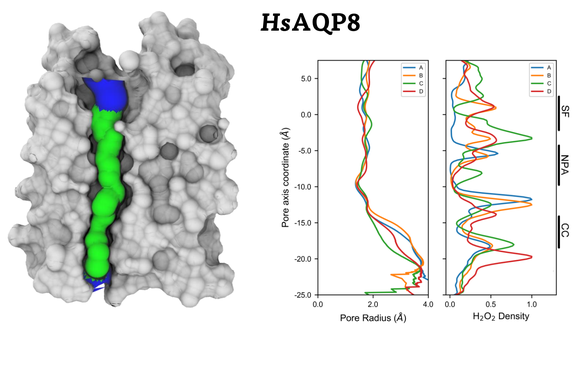

MIPs exhibiting positive experimental H_2O_2 transport

MIPs exhibiting negative experimental H_2O_2 transport

	MIP	H_2O_2 transport activity	Reference	Permeation events by chain
AQP1-LIKE	*Mt*PIP2;3	+	Chevriau *et al.*, 2024	11-4-0-5
	*Hs*AQP1	-	Almasalmeh *et al*, 2014	47-33-24-63
	*At*PIP2;4	+	Hooijmaijers *et al*, 2012	24-0-4-0
	*At*PIP2;8	-	Hooijmaijers *et al*, 2012	7-5-0-0
AQP3-LIKE	HsAQP3	+	Miller *et al*, 2010	25-10-9-11
	OsNIP3;3	+	Katsuhara *et al*, 2014	34-37-34-67
	OsNIP3;1	-	Katsuhara *et al*, 2014	62-53-53-34
AQP8-LIKE	HsAQP8	+	Almasalmeh *et al*, 2013 Laforenza *et al*, 2017	6-17-11-18
	AtTIP1;2	+	Bienert *et al*, 2007	19-17-22-21
	AtTIP2;1	-	Bienert *et al*, 2007	6-10-1-0
AQP11-LIKE	HsAQP11	+	Bestetti *et al*, 2019	303-91-83-49

Methods

Molecular Dynamics simulations
Molecular dynamics simulations were performed for homotetrameric assemblies of selected MIP, with homology models created with SWISS-MODEL online server, using SoPIP2;1 open state crystal 3D structure (2B5F) as template, or by AlphaFold Server. Assemblies were embedded in a fully hydrated POPC bilayer, with explicit solvent (TIP3P water) and ions (NaCl 0.15M) using the membrane builder tool provided in the CHARMM-GUI website. ~300mM was added to the systems by replacement of water molecules, and 500ns unbiased molecular dynamics simulations were run with in an NPT ensemble with full periodic boundary conditions, performed with AMBER18 MD package, using hydrogen mass repartitioning (HMR) and parameters from AMBER14SB and LIPID17 force fields.

Density probability calculation
The density probability function were calculated by extracting the XYZ positions of the geometric center of the H_2O_2 or H_2O molecules throughout the simulation time with the cpptraj program of the AmberTools package. The origin of the Z coordinate of the system was centered in each simulation frame towards the geometric center formed by the Ar/R residues and the probability density along the pore was calculated by Kernel Density Estimation (KDE) using the software R.

Permeation events
To quantify permeation events, a custom Python script was developed. This script leverages molecular dynamics trajectories to track the movement of molecules through a defined pore region. Specifically, the script establishes reference points on either side of the pore and counts the number of molecules that traverse these points over the course of the simulation, regardless of the direction of permeation.

Pore Dimensions
To calculate pore dimensions along the Z-axis for each trajectory and perform statistical analysis, the HOLE module within the MDAnalysis package was employed, along with custom Python scripts.

Conclusions

- Spontaneous H_2O_2 permeation was observed in channels previously considered non-transporters (AtPIP2;8, OsNIP3;1, AtTIP2;1). This suggests pore structure alone doesn't fully explain H_2O_2 permeability, with other factors like post-translational modifications, lipid interactions, or experimental limitations playing a role. Negative results in yeast experimental assays may be due to methodological issues.
- H_2O_2 transport appears to be a characteristic shared across multiple MIP families, suggesting it could be an ancestral trait. The loss of H_2O_2 permeability in certain MIPs may not be due to changes in the pore itself, but rather to post-translational modifications or regulatory mechanisms acting outside the pore.
- The H_2O_2 restriction seen in *Mt*PIP2;3 NPA region was also observed in other MIP families, indicating this may be a broader regulatory mechanism.

References
- Almasalmeh et al. (2014). **FEBS Journal, 281(3),** 647–656. https://doi.org/10.1111/febs.12653
- Bestetti et al. (2019). **Redox Biology, 28,** 101326. https://doi.org/10.1016/j.redox.2019.101326
- Bienert et al. (2007). **Journal of Biological Chemistry, 282(2),** 1183–1192. https://doi.org/10.1074/jbc.M603761200
- Chevriau et al. (2024). **Biochemical Journal.** https://doi.org/10.1042/bcj20240310
- Hooijmaijers et al. (2012). **Journal of Plant Research, 125(1),** 147–153. https://doi.org/10.1007/s10265-011-0413-2
- Katsuhara et al. (2014). **Plant Biotechnology, 31(3),** 213–219. https://doi.org/10.5511/plantbiotechnology.14.0421a
- Laforenza et al. (2016). **International Journal of Molecular Sciences, 18(1),** 66. https://doi.org/10.3390/ijms18010066
- Miller et al. (2010). **PNAS, 107(36),** 15681–15686. https://doi.org/10.1073/pnas.1005776107

Acknowledgement and/or funding:
Fundings KA: ANPyCT (PICT2019-2019-00387, PICT2021-I-A-00040); CONICET (PIP-11220210100099CO) ; UBA (UBACYT-2023).
GZDP: ANPyCT (PICTO-UNAHUR 2019-0023).
Thanks to NVIDIA for Titan V GPU grant.
This work used computational resources from CCAD-UNC, which is part of SNCAD-MinCyT, Argentina.